Peer-reviewed version available at Metals 2019, 9, 158; doi:10.3390/met9020158

Article

Control Upstream Austenite Grain Coarsening during Thin Slab Casting Direct Rolling (TSCDR) Process

Tihe Zhou [1,*], Ronald J. O`Malley [2], Hatem S. Zurob [1], Mani Subramanian [1], Sang-Hyun Cho [3], and Peng Zhang [3]

[1] Department of Materials Science and Engineering, McMaster University, 1280 Main Street West, Hamilton L8S 4L7, Ontario, Canada; tom.zhou@stelco.com; zurobh@mcmaster.ca (H.S.Z.); subraman@mcmaster.ca (M.S.)

[2] Department of Materials Science and Engineering, Missouri University of Science & Technology, 1400 N. Bishop Ave., Rolla 65409-0330, MO, USA; omalleyr@mst.edu (R.J. O'M.)

[3] Algoma Inc. 105 West Street, Sault Ste. Marie, Ontario P6A 7B4, Canada; Sang-Hyun.Cho@algoma.com (S.-H.C.); peng.zhang@algoma.com (P.Z.)

* Correspondence: tom.zhou@stelco.com; Tel.: +1-519-587-4541 ext. 5398

Abstract: Thin Slab Casting and Directing Rolling (TSCDR) has become a major process for flat-rolled production. However, the elimination of slab reheating and limited number of thermomechanical deformation passes leave fewer opportunities for austenite grain refinement resulting in some large grains persist in the final microstructure. In order to achieve excellent Ductile to Brittle Transition Temperature (DBTT) and Drop Weight Tear Test (DWTT) properties in thicker gauge high strength low alloy products, it is necessary to control austenite grain coarsening prior to the onset of thermomechanical processing. This contribution proposes a suite of methods to refine the austenite grain from both theoretical and practical perspective including: increasing cooling rate during casting, liquid core reduction, increasing austenite nucleation sites during the delta ferrite to austenite phase transformation, controlling holding furnace temperature and time to avoid austenite coarsening, and producing new alloy with two phase pinning to arrest grain coarsening. These methodologies can not only refine austenite grain size in the slab center, but also improve the slab homogeneity.

Keywords: thin slab casting direct rolling; austenite grain coarsening; grain growth control; liquid core reduction; secondary cooling; two phase pinning

1. Introduction

Owing to low capital and operating cost, Thin Slab Casting and Directing Rolling (TSCDR) has become a major process for hot flat-rolled production since Nucor started the first thin slab caster directly linked to a hot rolling mill back to 1989. This process is based on a novel funnel mould caster which can produce a thin slab of thickness from 50 to 90 mm, instead of the conventional continuous casting slab thicknesses of 200 to 250 mm [1,2]. Figure 1 is an example of the TSCDR process at Algoma Inc. The liquid steel is fed via the ladle and tundish into a funnel-shaped copper mould with primary cooling control. Solidification initiates on the mould wall and the external solidified shell increases in thickness as the steel strand passes through the mould. Based on the steel grades and slab thickness, the casting speed can be from 2.5 to 6.5 m/min. Once leaving the mould, the thin slab passes through the secondary-cooling-zone and solidification continues. The secondary-cooling zone has eight segments with multi-point bending and unbending with 12.7-meter containment length by using air mist cooling. The liquid core reduction system can refine the as-cast microstructure and reduce the centerline segregation and solidification related defects. The

Peer-reviewed version available at Metals 2019, 9, 158; doi:10.3390/met9020158

continuous slab is cut to length and then sent to the roller hearth soaking furnace. To maximize the use of the rolling capacity, the thin slab caster has two strands along with two shuttle furnaces which can transfer the slab sideways to allow the two strands to feed a single rolling mill. The slab is rolled in a single pass roughing mill after descaling, then goes through the heated transfer table and is rolled in the six-stand finishing mill; the resulting hot strip then passes through the run-out table with a laminar cooling system and is coiled at the down coiler [3].

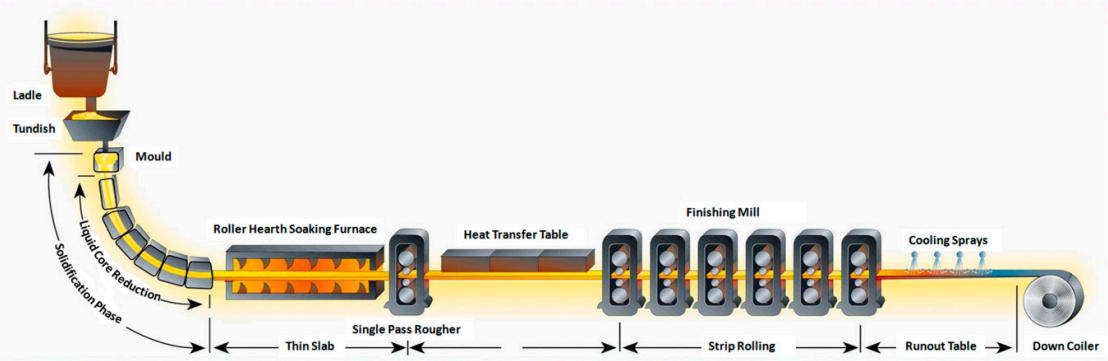

Figure 1. Thin Slab Casting Direct Strip Production Complex at Algoma Inc. [3].

TSCDR mills currently produce a variety steel grades including interstitial free steel, low carbon to medium carbon steel, high-strength low-alloy and advanced high strength multiphase steel grades [1]. Recently great effort has been placed on using this process to produce high grade microalloyed steels that can be utilized in bridge guard rail, wind turbine towers, rail car and oil & gas industrial with stringent low temperature Ductile to Brittle Transition (DBTT) and Drop Weight Tear Test (DWTT) requirements to maintain structural integrity and safety over several decades of service [4,5]. It well established that refining austenite grain size before pancaking can improve DBTT and DWTT properties [6]. In most cases, these applications require a hot band thickness of 10mm or more. This requirement challenges the TSCDR process because the ratio of the thickness of the initial as-cast slab to that of the final product is only of the order of 5–7 to 1. It has been proven that production of higher HSLA grades is very difficult owing to the presence of extremely large austenite grains in the center of the slab prior to thermomechanical processing [7]. The limited number of thermomechanical deformation passes available in the TSCDR process cannot refine these larger grains [8,9]. In order to achieve uniform and finer microstructure, it is very important to control the upstream austenite grain coarsening before the slab enters the roughing mill. This contribution will focus on refining austenite grain by increasing the cooling rate during solidification, increasing nucleation sites for delta ferrite by liquid core reduction and increasing austenite nucleation sites during the delta ferrite to austenite phase transformation, as well as controlling austenite coarsening inside the holding furnace. In addition, the possibility of rolling new alloy with two phase pinning is also discussed.

2. Materials, Experimental Procedure and Model Setup

The experimental materials in this study consist of an HSLA based API X70 cast slab sample from industry, as well as an Fe-Al model alloy with 1.5% Al addition to generate delta/austenite two-phase microstructure at different temperatures. The two chemistries are compared in Table 1. The addition of Al in the Fe-Al model alloy can stabilize delta-ferrite down to room temperature. A two-phase mixture of delta ferrite and austenite will exist at temperatures between 1310 °C and the eutectoid temperature. The Fe-Al model alloy was prepared by induction melting at CANMET Materials Technology Lab (Hamilton, Canada); the as-received microstructure is delta-ferrite with grain size of approximately 85 μm after pilot mill hot rolling to the thickness of 10mm

Table 1. Chemical composition of the new alloy used in this investigation (wt %).

wt %	C	Mn	Si	Al	Ti	Nb	N
API X70	0.05	1.60	0.30	0.0037	0.0012	0.07	0.0060
Fe-1.5Al% model alloy	0.051	1.00	0.36	1.5	0	0	0

In order to quantify the grain coarsening at high temperature, a simple non-isothermal grain growth model [9] is utilized to capture the evolution of grain growth at different stages of TSCDR process. Starting with the simple equation:

$$\frac{d\bar{R}}{dt} = \alpha M(t)\frac{2\gamma_{gb}}{\bar{R}} \quad (1)$$

then integrating with respect to time, leads to:

$$\bar{R}^2 = \bar{R}_0^2 + 4\gamma_{gb}\int_0^t \alpha M(t)dt \quad (2)$$

where $\bar{R}$ is the mean radius of an individual grain, $\bar{R}_0$ is the initial grain radius, and γ_{gb} denotes the grain boundary energy per unit of area, a reasonable value of 0.8 J·m^{-2} [10] is used for the calculation. α is a shape factor with value of ~1.5 [11], and $M(t)$ is the mobility of the grain boundaries [9,12]. Delta ferrite grain boundary mobility is shown as [9]:

$$M_\delta(t) = \frac{0.7075}{T(t)} \times \exp\left(\frac{-20,995.43}{T(t)}\right) \quad (3)$$

While austenite grain boundary mobility is listed as [9]:

$$M_\gamma(t) = \frac{0.3072}{T(t)} \times \exp\left(\frac{-20,837.14}{T(t)}\right) \quad (4)$$

In this equation $T(t)$ is an expression for the temperature as a function of time which was obtained either experimentally from the data recorded using a thermocouple or heat transfer model predicted temperature profiles during the TSCDR process.

During a typical TSCDR practice, for instance, Table 1 chemistry, Ti concentration is very low and large TiN particles are formed in the liquid during the late stages of solidification. These particles coarsen during subsequent solid state process at high temperature [13,14]. These large TiN particles exert a very small particle pinning effect [15]. Strong particle pinning conditions are not encountered until fine Nb(C,N) precipitates are formed during thermomechanical processing [16–18]. In addition, according to Zurob et al [19], the solute-drag effect of all alloying elements was shown to be negligible at temperatures above 1200 °C. Therefore, Equation (2) can be used to model the grain-size evolution during the TSCDR process up to the point where the slabs exit the homogenization furnace prior to thermomechanical processing at the roughing mill.

To validate the grain growth model, a 70 and an 85 mm thickness slab of APIX70 were sampled after solidification prior to entering the twin roller hearth tunnel furnaces. The slab crops were sectioned to measure the austenite grain size at various distances from the slab surface. All the samples were prepared using standard metallographic techniques. The prior austenite grain boundaries were revealed using an aqueous solution of picric acid with sodium dodecylbenzene sulfonate with additions of hydrochloric acid for the different chemistry. Microstructure was investigated using optical and scanning electron microscopy. The image analysis was performed using Clemex PE5.0 software. The grain size was measured using the area intercept method and the true three-dimensional grain diameter was calculated as 1.382 times the linear intercept diameter [20].

3. Results and Discussions

3.1. Microstructure and Model Validation

The microstructure of the industrially supplied TSCDR 85 and 70 mm thick slabs of API X70 steel are shown in Figures 2 and 3 respectively. At the surface of the 85 mm APIX70 slab, the prior austenite grain size is about 50 μm. At the centre of the slab, the prior austenite grain size is as large as 1151 μm. While, the prior austenite grain size at the surface of the 70 mm APIX70 slab is about 14 μm, and at the center of the slab is about 858 μm.

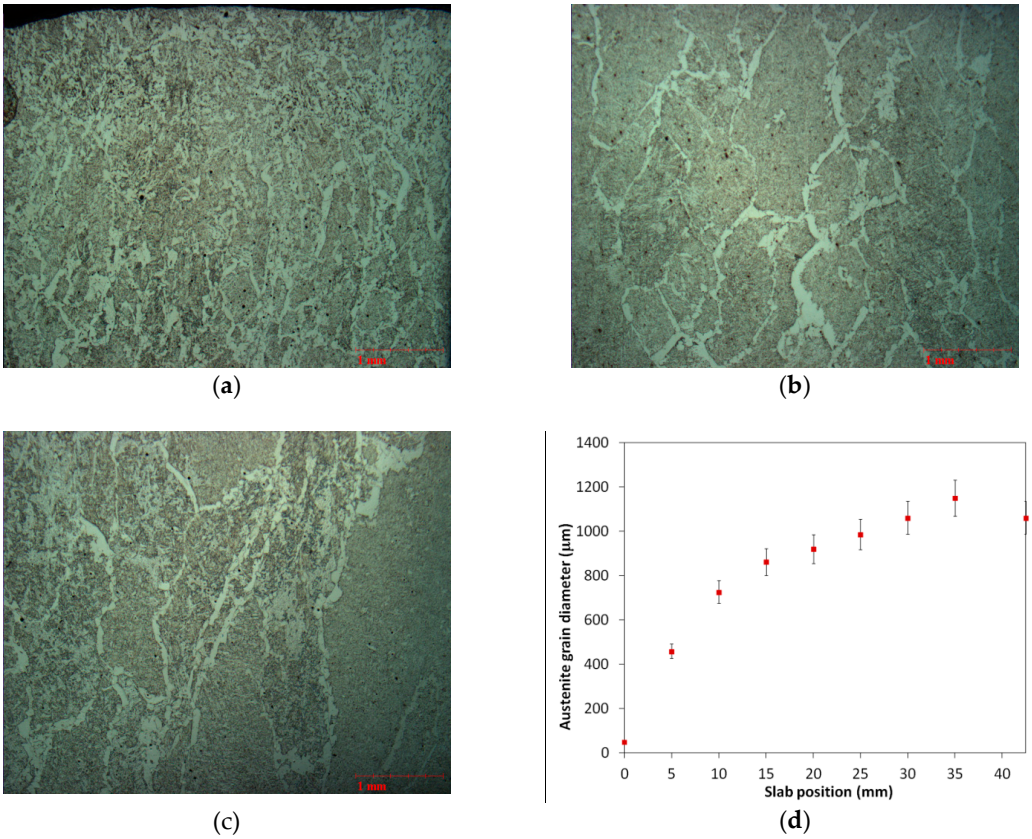

Figure 2. 85 mm slab austenite grain size evolution of API X70 from industrial thin slab casting process (**a**) close to slab surface, (**b**) 20 mm from the slab surface, (**c**) close to the slab center, and (**d**) summary of the measured austenite grain size with distance from slab surface to center.

Figures 2 and 3 indicated that the industrial TSCDR as-cast microstructure is non-uniform with extremely large grains at the slab centre, and that the 70 mm thick slab has a finer austenite grain size compared to 80 mm slab.

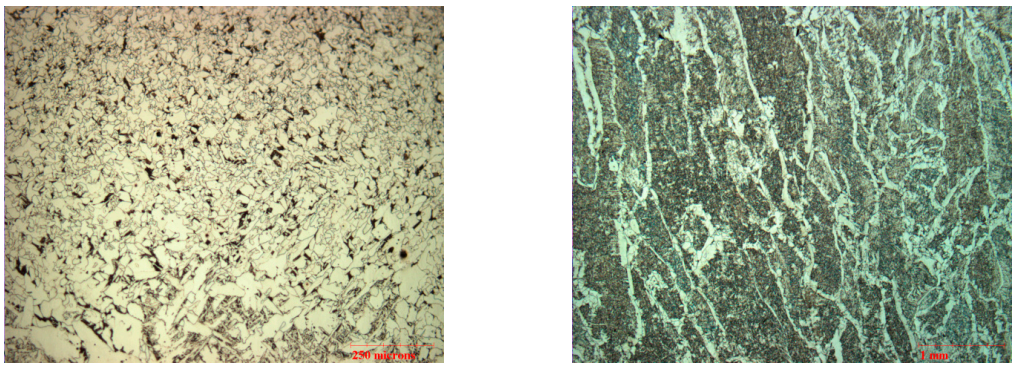

Preprints (www.preprints.org) | NOT PEER-REVIEWED | Posted: 23 January 2019 doi:10.20944/preprints201901.0230.v1

Peer-reviewed version available at Metals 2019, 9, 158; doi:10.3390/met9020158

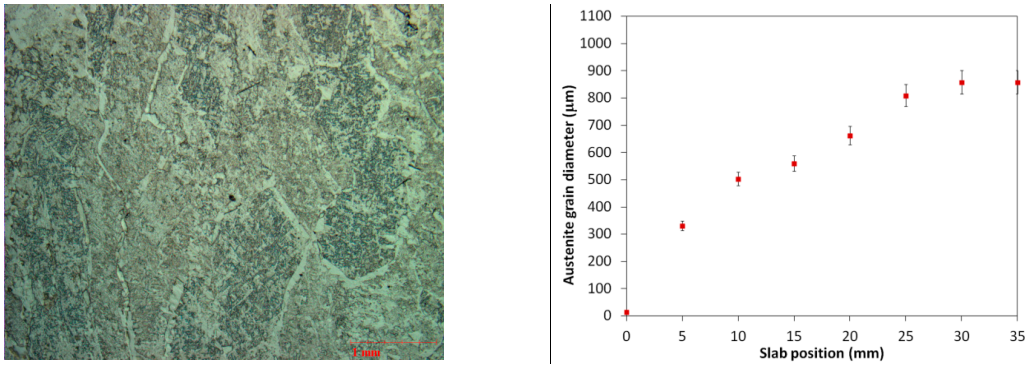

(**c**) (**d**)

Figure 3. 70 mm slab austenite grain size evolution of APIX70 from industrial thin slab casting process (**a**) close to slab surface, (**b**) 20 mm from the slab surface, (**c**) close to the slab center, and (**d**) summary of the measured austenite grain size with distance from slab surface to center.

The grain growth model Equation (2) can be used to calculate the delta ferrite and austenite grain size evolution at different positions in the slab. The important points that require to be considered is that the initial grain size $\bar{R}_0$ and the cooling path ($T(t)$ in Equations (3) and (4)) varies from the surface to the center of the slab, leading to grain-size variations. To understand the HSLA microstructure evolution during the TSCDR process, THERMO-CALC is used to predict the relevant transformation temperatures for API X70 and Fe-Al model alloy using the TCFE6 database [21]. The results are given in Table 2.

Table 2. Phase transformation temperature of APIX 70.

Phase	Liquid	Liquid + Delta	Delta	Delta + Austenite	Austenite
APIX 70 (°C)	>1524	1524–1496	1496–1477	1477–1448	1448–852
Fe-Al alloy (°C)	>1530	1530–1500	1500–1412	1412–734	

In this study, we have not attempted to model the delta ferrite to austenite transformation. Instead we simply assumed that the delta grain growth occurs down to 1477 °C and austenite grain growth occurs after the delta ferrite to austenite phase transformation. The secondary dendrite arm spacing (SDAS) is used as the initial delta-ferrite grain size, $\bar{R}_0$, which was calculated using CON1D V7.0 slab casting heat transfer model assuming the casting speed of 3.4 meter per minute [22], as shown in Figure 4a. The initial austenite grain size was presumed to be smaller than the final delta grain size and was divided by a factor of 3 [23,24] to account for the effect of grain refinement due to the delta-ferrite to austenite transformation in the grain size calculation. Finally, the cooling path $T(t)$ at each point of the slab is also estimated by CON1D V7.0 model [22]. For example, Figure 4b shows the temperature paths at the surface, 5 mm, 10 mm, 20 mm, 30 mm below the surface, and the center of API X70 85 mm slab that was cast with 3.4 m/min casting speed. Due to the spay jet cooling and the high local heat extraction when the segment rolls directly contact the slab, the temperature curve on the slab surface shows irregular trend. Nonetheless, this irregular trend should not interfere with the interpretation of the grain growth with the slab position during the TSCDR process.

Preprints (www.preprints.org) | NOT PEER-REVIEWED | Posted: 23 January 2019 doi:10.20944/preprints201901.0230.v1

Peer-reviewed version available at Metals 2019, 9, 158; doi:10.3390/met9020158

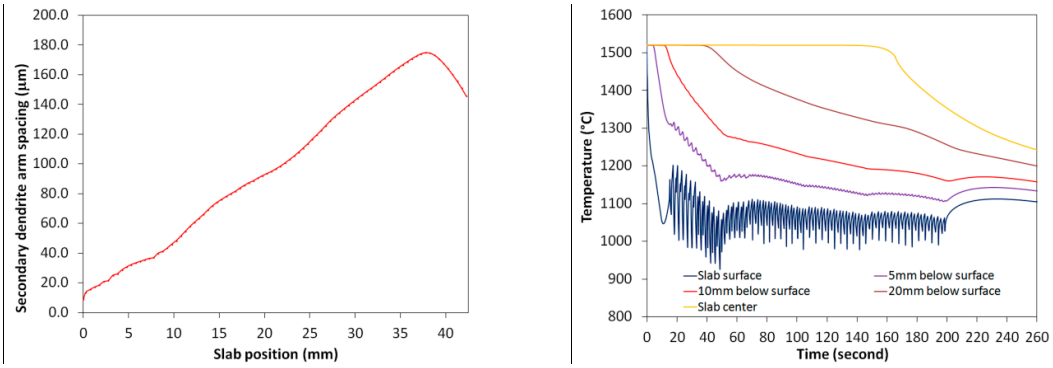

(**a**) (**b**)

Figure 4. CON1D V7.0 Slab Casting Heat Transfer model predicted (**a**) secondary dendrite arm spacing as a function of position within the APIX70 slab, (**b**) temperature paths at the surface, 5 mm, 10 mm, 20 mm, the surface and the centre of the slab.

Using Equations (2) and (3), an example of delta grain size evolution with time at 5 mm below the slab surface is shown in Figure 5a. The austenite grain size evolution at the same position (5 mm below the surface) with time just before leaving the holding furnace by using Equations (2) and (4) is shown in Figure 5b. The solid line represents the model predicted austenite grain diameter and the dashed line represents the temperature profile in the TSCDR process at the corresponding slab position.

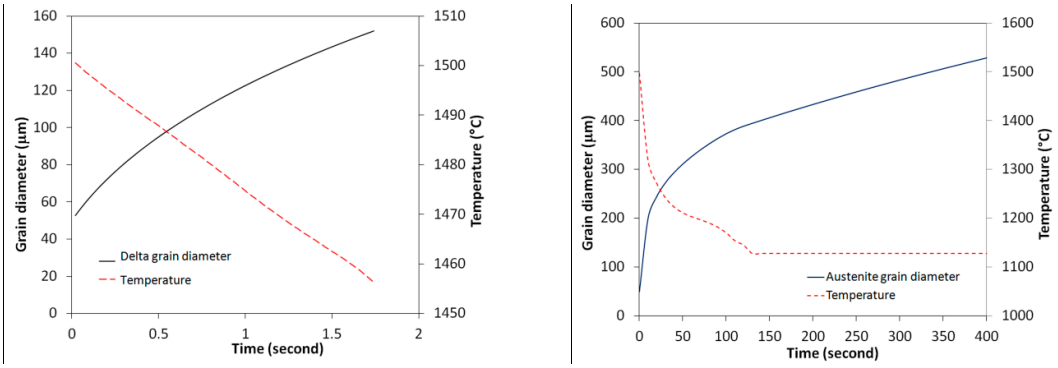

(**a**) (**b**)

Figure 5. (**a**) The predicted delta grain size evolution with time 5 mm below the slab surface, and (**b**) the predicted austenite grain size evolution at the same position before entering the roller hearth holding furnace.

Similar calculations were conducted as a function of the slab thickness. Figure 6a shows the predicted delta grain size as a function of slab position, just before the onset of the delta ferrite to austenite transformation. The solid diamonds are the calculated delta grain sizes; the solid line is used to highlight the trends of grain size change with distance from the surface to center of the slab. In addition, the austenite grain size can be calculated when the slab is about to enter the holding furnace, and upon leaving the holding furnace prior to entering roughing mill.

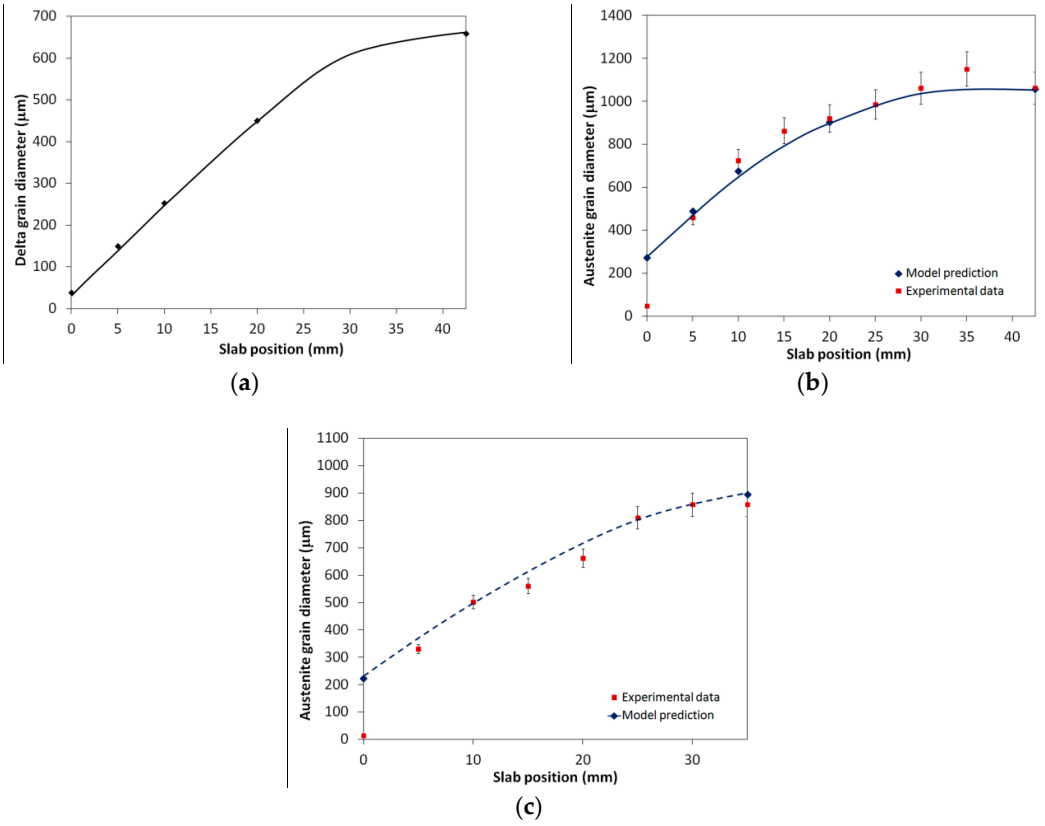

Figure 6. (**a**) The predicted delta grain size as a function of slab position, (**b**) Comparison of model calculated and experimental measurement of austenite grain size with slab position before the 85mm slab entering the holding furnace, and (**c**) comparison of model calculated and experimental measurement of austenite grain size with slab position before the 70 mm slab entering the holding furnace.

Figure 6b shows the calculated austenite grain size with slab thickness when the slab is about to enter the holding furnace. The solid diamonds and solid lines follow the same notation for delta grains as noted previously. The experimentally measured austenite grain size from 85 mm slab from Figure 2d (solid squares) is superimposed for comparison. It indicates that very good agreement is obtained between the model predicted and measured austenite grain size as a function of slab position. This provides strong support that the normal grain growth model developed here can be used to predict austenite grain growth at high temperatures prior to the thermomechanical processing. The calculated austenite grain size for the 70 mm slab and the corresponding experimental measurements (Figure 3d) with slab position is shown in Figure 6c. Once again, the predicted austenite grain size is in good agreement with the experimental data as a function of slab position. This agreement further validates the grain growth treatment employed here and supports the applications of model in the following sections.

3.2. Increasing Cooling Rate to Refine as-Cast Microstructure

Reducing the slab thickness can increase the cooling rate at the slab center, which can refine the austenite grain at the slab center and reduce the non-uniformity of the as-cast microstructure. In what follows, the consequences of reducing the slab thickness from 85 mm to 50 mm and 30 mm are examined assuming that the only change is the enhanced cooling rate of the slab [25–27]. In order to determine the cooling rate and the initial secondary dendrite arm spacing, the CON1D V7.0 Slab Casting Heat Transfer Model [22] was used for slabs of 85 mm, 50 mm and 30 mm slab thickness as shown in Figure 7.

Preprints (www.preprints.org) | NOT PEER-REVIEWED | Posted: 23 January 2019 doi:10.20944/preprints201901.0230.v1

Peer-reviewed version available at Metals 2019, 9, 158; doi:10.3390/met9020158

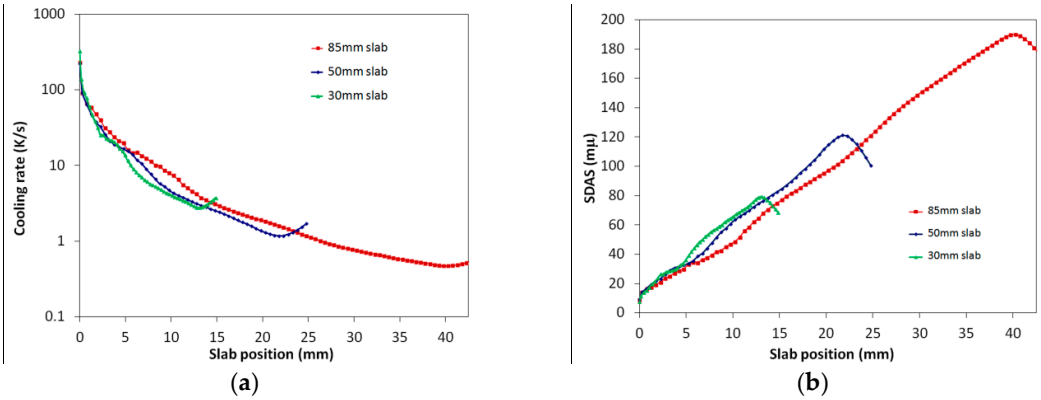

(**a**) (**b**)

Figure 7. CON1D V7.0 Slab Casting Heat Transfer model predicted (**a**) Cooling curves and (**b**) SDAS at different position of 30 mm, 50 mm and 85 mm slab.

The initial delta-ferrite grain size was, once again, taken to be SDAS, therefore, the model calculated of delta grain size as a function of position for the 30 mm, 50 mm thin slab just before the onset of the delta to gamma transformation are shown in Figure 8a, which also includes, for comparison, the results shown earlier for the 70mm and 85 mm slab. The calculated austenite grain size before entering the homogenization furnace is shown in Figure 8b. The symbols in these Figures have the same meaning as discussed previously.

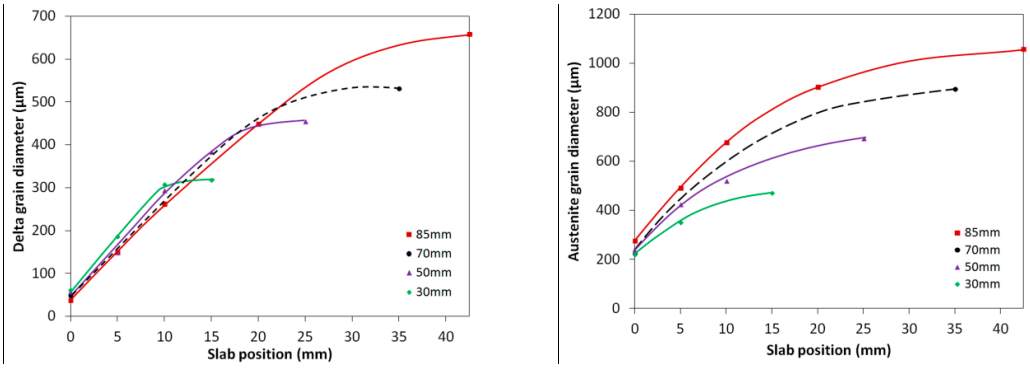

(**a**) (**b**)

Figure 8. (**a**) The predicted delta grain size of 30 mm, 50 mm, 70mm and 85 mm slab as a function of slab position just before the onset of the delta to gamma transformation, (**b**) the predicted austenite grain size of 85 mm, 70mm, 50 mm and 30 mm slab as a function of slab position when the slab is about to enter the homogenization furnace.

It is clear from these calculations that by the enhanced cooling rate, austenite grains at the centre of the thinner slabs have greatly reduced in size. When the slabs are about to enter the homogenization furnace, the austenite grain size at the center of an 85 mm thick slab is about 1058 μm. However, the grain size is 896 μm at a 70 mm thick slab, the grain size is 693 μm at a 50 mm thick slab and 470 μm for a 30 mm slab. In addition, the homogeneity of the microstructure has improved by increasing the cooling rate; the ratio of largest grain size to smallest grain size is 3.8 to 1 for an 85 mm thick slab, 2.8 to 1 for a 50 mm thick slab and 2.1 to 1 for a 30 mm slab. Therefore, one can conclude that reducing the slab thickness can refine and homogenize the as-cast microstructure due to the enhanced cooling rate at the centre of the slab. Experimental measurement of 85mm (Figure 2) and 70mm (Figure 3) industrial slab austenite grain size with the distance from the slab surface to center demonstrated the validity and technological merit of the increasing cooling on reducing austenite grains at the center of the slab: The austenite grain size can be reduced from 1151 μm to 858 μm if the casting slab thickness is reduced from 85mm to 70mm. The main difficulty in

Preprints (www.preprints.org) | NOT PEER-REVIEWED | Posted: 23 January 2019 doi:10.20944/preprints201901.0230.v1

Peer-reviewed version available at Metals 2019, 9, 158; doi:10.3390/met9020158

applying this method is that it requires changing the layout of the TSCDR process for casting thinner slab susch as 50mm and 30mm thich slab. In addition, the smaller slab thickness will further reduce the amount of thermomechanical processing that can be performed downstream resulting in a larger average grain size and possibly more grain size non-uniformity despite the improved initial microstructure. Thus, an optimum thickness could be determined by considering both the solidification and grain growth (as described above) as well as the subsequent thermomechanical processing.

It is well established that as-cast microstructure is a function of the solidification rate (V) and temperature gradient (G) ahead of the solid-liquid front. The effect of the temperature gradient and velocity on the primary dendrite arm spacing can be summarized in the following equation [30,31]:

$$\lambda_1 = A_1 G^{-m} V^{-n} \quad (5)$$

where λ_1 is the primary arm spacing, G is the average temperature gradient in front of tip of dendrite in the liquid side, V is average solidification velocity. A_1, m and n are constants. For the second dendrite arm spacing λ_2, the most widely accepted expression for the relationship between λ_2 and cooling rate (GV) [32,33]:

$$\lambda_2 = B_1 (GV)^{-n} \quad (6)$$

where B_1 and n are constants. Increasing secondary cooling with restricted casting speed will increase cooling rate (GV). As a result, the primary and second dendrite arm spacing will decrease based on Equations (5) and (6). Figure 12a for the Algoma DSPC model predicted slab surface temperatures using different secondary cooling set-ups (the water loops configuration of DSPC is illustrated in Figure 12b). The solid diamonds are the slab surface temperatures for the standard spray cooling set-up used for low carbon steels, 0.6 l/kg of hot steel, and the increased secondary cooling, 1.4 l/kg of hot steel, is used for HSLA steels (solid squares in Figure 9a). When the liquid superheat is above 15°C, the casting speed is restricted to 3.0 m/min; once the liquid superheat is below 10 °C, the casting speed can be increased to 3.4 m/min. Based on the above setup, the predicted 85 mm slab surface and center temperature profiles using increased secondary cooling with a casting speed 3.0 m/min using the CON1D V7.0 model are shown in Figure 9c. Figure 9d shows austenite grain size with slab position using standard cooling and increased secondary cooling. The solid line highlights the trends of grain refinement with distance from the slab surface to the center. The increased secondary cooling practice is predicted to have a much finer austenite grain size than the standard spray practice at both the surface and center of the slab: austenite grain size is reduced from 276 μm to 253 μm at surface and from 1058 μm m to 808 μm m in the slab center.

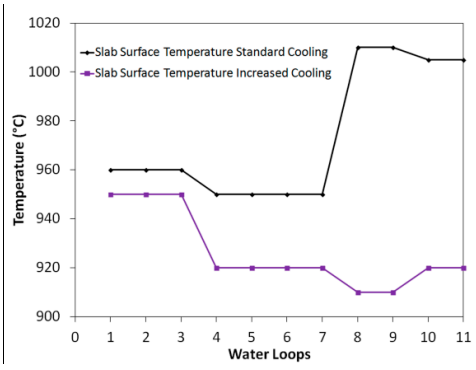

(**a**)

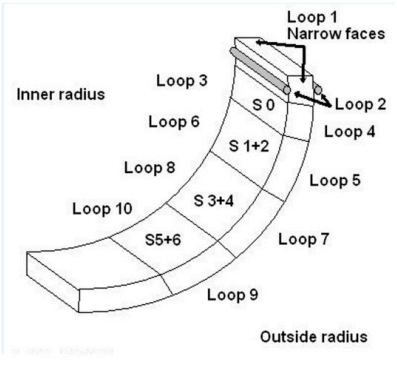

(**b**)

Preprints (www.preprints.org) | NOT PEER-REVIEWED | Posted: 23 January 2019 doi:10.20944/preprints201901.0230.v1

Peer-reviewed version available at Metals 2019, 9, 158; doi:10.3390/met9020158

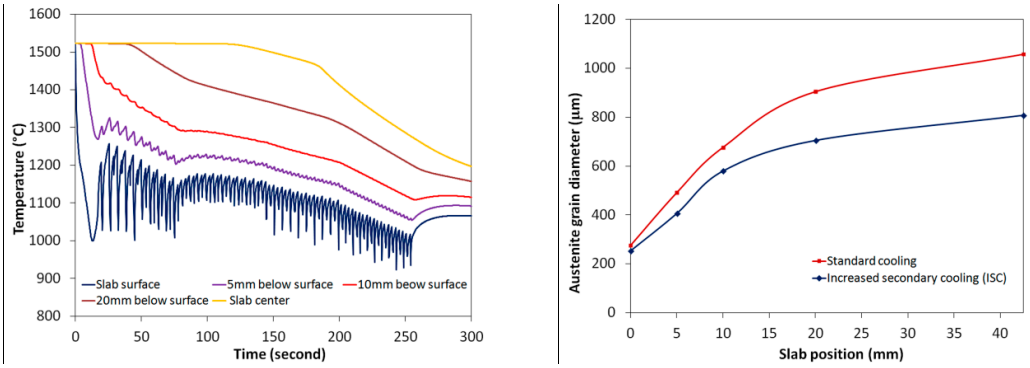

(c) (d)

Figure 9. (**a**) Measured slab surface temperature using different secondary cooling set-up, (**b**) the water loops configuration at Algoma DSPC, (**c**) calculated the 85mm slab temperature profile using increased secondary cooling, and (**d**) comparison of 85mm slab austenite grain size using standard cooling and increased secondary cooling.

3.3. Liquid Core Reduction

The TSCDR process at Algoma Inc. can adjust the strand gap dynamically during the casting process. The strand thickness can be reduced just below the mould by a tapered roll guide configuration of the "0" segment. Approximately a 10–30 mm strand reduction can be achieved with liquid core by means of many hydraulically adjustable roll support segments. In this way, the slab thickness can be reduced from 98 mm to either 85 or 70 mm (Figure 10a). The liquid core reduction during casting produces a convective movement which mixes the solidified dendrite structure and the liquid steel. A melt flow introduced by convection will generate strong shear stresses, which will shed away the newly formed dendrite arms near the solidification front. The newly formed dendrite crystals are then transported into the hot liquid pool by convective movement. Some of the dendrites are remelted while others survive and are transported back to the solidifying region. These surviving broken dendrite tips then form additional nucleation sites for delta ferrite [28]. The finer delta ferrite, in turn, will provide more nucleation sites for austenite during the delta ferrite to austenite phase transformation resulting austenite grain refinement. This basic grain multiplication mechanism induced by liquid core reductions is shown schematically in Figure 10b.

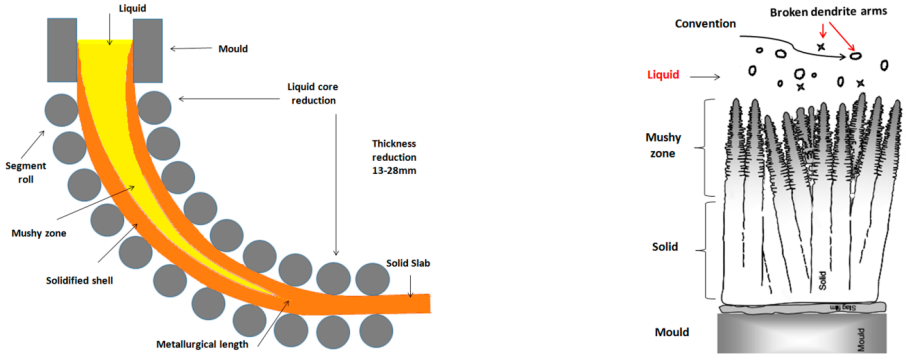

(a) (b)

Figure 10. (**a**) Sketch diagram of liquid core reduction during TSCDR process, (**b**) The basic mechanism of grain multiplication or grain refinement from liquid core reduction in the solidification region. The convective movement generates shear to break the dendrite tips and circulates the debris in the liquid pool.

The liquid core reduction can not only refine as cast microstructure, but also can reduce center line segregation, as well as other solidification defects such as shrinkages and porosity. The

metallurgical length for HSLA steels is about 10.0 m which is at the end of segment "6". The liquid core reduction system together with a dynamic control of the liquid pool length can predict the best squeezing point during casting these HSLA grades. For APIX70, the liquid core reduction is set is to occur at the fraction solid of between 0.4–0.6. Figure 11a,b show API chemistry slab macro etch from strand 3 and strand 4 at the slab center position respectively. The strand #3 slab sample shows centerline segregation and solidification shrinkages which indicates that the squeezing was done late with higher solid fraction, however, the strand 4 sample has the diffused centerline which confirms that the liquid core reduction was carried out at the optimum set point in solid fraction.

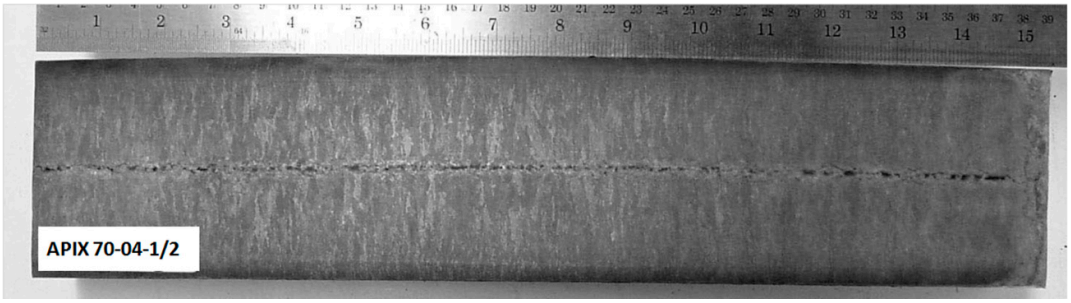

(**a**)

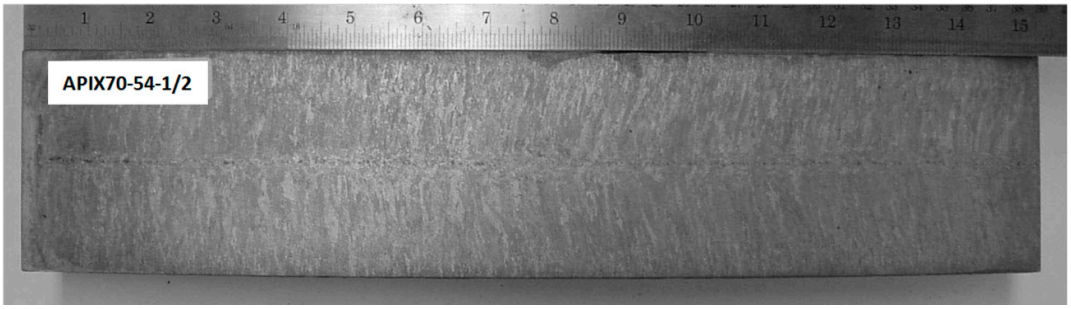

(**b**)

Figure 11. API X70 slab macroetch from (**a**) strand 3 and (**b**) strand 4 with different set point of liquid core reduction.

3.4. Increasing the Number of Austenite Nucleation Sites during Delta-Ferrite to Austenite Phase Transformation

The HSLA steels are low carbon steels (<0.08 wt %) which solidify as delta ferrite. The ThermoCalc predicted the delta to austenite phase transformation is about 1477 °C (Table 2) and occurs during the liquid core reduction stage. Very little information is available concerning the kinetics of this transformation and its effect on the grain size. To demonstrate the refinement of as-cast microstructure using deformation, the Fe-Al model alloy (Table 1) was studied using a quenching dilatometer at CANMET Materials Technology Lab [29]. Microstructure of specimen reheated into the delta region and after holding for 60 s, a compressive strain of 0.2 was applied followed cooling at 50 °C/s to 1125 °C) is shown in Figure 12. Figure 12a shows fine sub-grains present within the original delta ferrite grains. Higher magnification SEM image (Figure 12(b)) confirms that the sub-boundaries and the grain boundaries are decorated by fine austenite precipitates. Figure 12c electron backscatter diffraction (EBSD) map shows austenite grains nucleate along the delta grain and subgrain boundaries (red line is large angle grain boundary ($\theta > 12°$) and the white is low angle grain boundary ($12° > \theta > 2°$)). This demonstration suggests that sub-grains formed as a result of deformation prior to the delta to austenite transformation. During this phase transformation, the subgrain boundaries and the original delta grain boundaries provide nucleation sites for austenite grains, which will lead to refinement of the austenite grain structure.

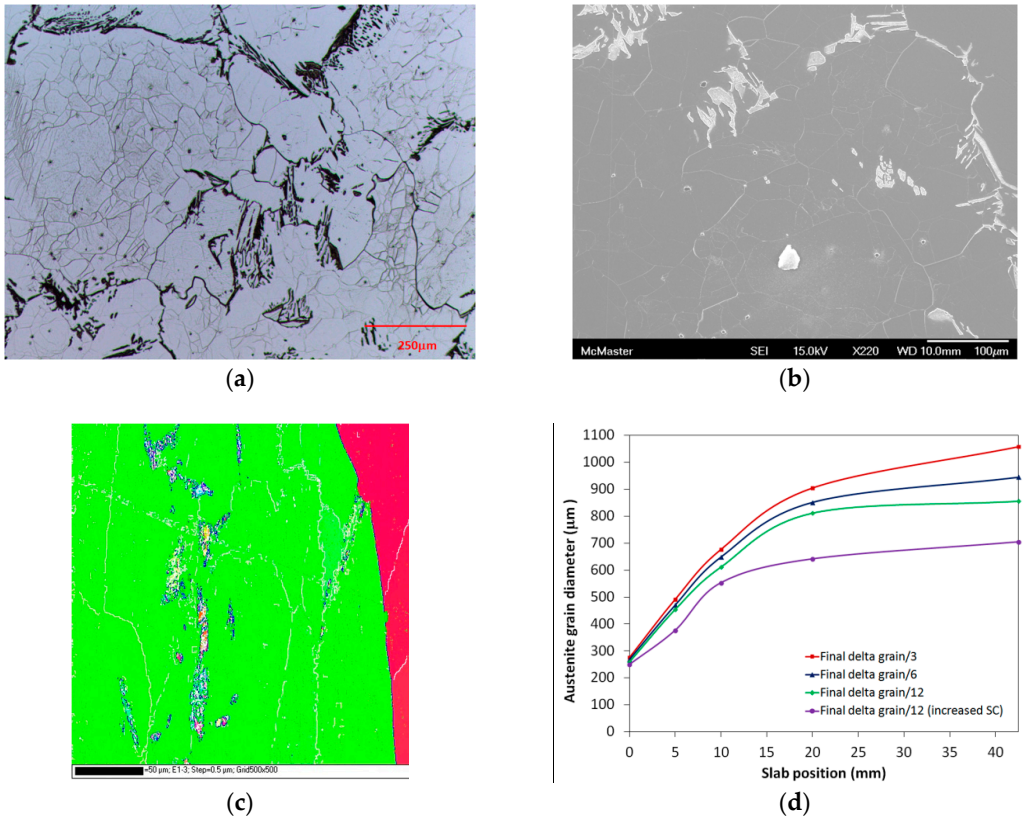

Figure 12. Microstructure of model Fe-Al ally reheated into the delta region, and after holding for 60 s, a compressive of 0.2 strain was applied followed cooling at 50 °C/s to 1125 °C: (**a**) the sample was quenched to room temperature as soon as it reached a temperature of 1125 °C, (**b**) austenite nucleates along the original delta grain boundaries, (**c**) EBSD shows austenite grains nucleate along the delta grain and subgrain boundaries, and (**d**) predicted austenite grain size when the slab is about to enter the homogenization furnace with different austenite nucleation sites.

To capture the effect of austenite nucleation sites on the austenite grain coarsening kinetics, the validated grain growth model can be used to calculate austenite grain evolution at different stage of TSCDR process. Figure 12d summarizes the predicted austenite grain size when the slab is about to enter the holding furnace for a different density of austenite nucleation sites. The various lines represent the grain size achieved when 12, 6, and 3 austenite grains nucleate within each delta grain. The calculation reveals that these extra nucleation sites have little effect on the final grain size at the surface of the slab, however, the austenite grain do decrease with increasing the austenite nucleation sites: the austenite grain in the 85 mm slab center can be reduced from 1058 µm to 945 µm and 856 µm respectively. The purple line in Figure 12d indicates austenite grain size trend by using the austenite nucleation density 12 and increased secondary cooling. The austenite grain size in the slab center can be refined from 1058 µm to 705 µm. The calculated results predicted the potential of increasing the number of austenite nucleation sites during delta-ferrite to austenite phase transformation to refine austenite grain size, much work still needed, however, to design new alloys and deformation schedule during casting that could take advantages of this novel approach.

3.5 Control of Holding Furnace Temperature and Holding Time:

Once the continuous slab leaves the secondary cooling zone, it is cut to length and then sent to the roller hearth holding furnace waiting for thermomechanical processing. The holding furnace standard set-up for HSLA at Algoma DSPC is holding temperature 1150 °C for 18 min. Austenite grains continue to coarsen inside the holding furnace. The experimental measurement of austenite

Preprints (www.preprints.org) | NOT PEER-REVIEWED | Posted: 23 January 2019 doi:10.20944/preprints201901.0230.v1

Peer-reviewed version available at Metals 2019, 9, 158; doi:10.3390/met9020158

grain size from 85 mm and 70 mm slab (Figure 2d and Figure 3d) are used as initial grain size, and the effects of holding temperature and time on austenite grain coarsening by using Equations (2) and (4) are summarized in Figure 13.

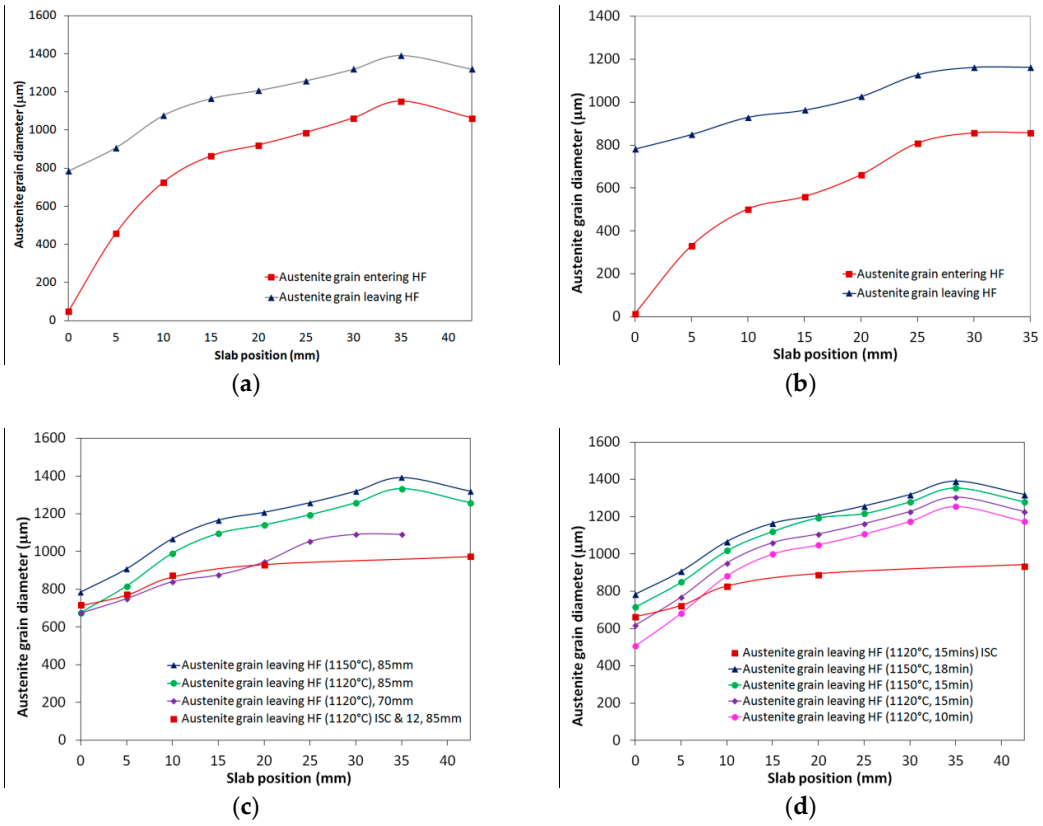

Figure 13. (**a**) Comparison of DSPC 85 mm austenite grain size before entering and after leaving the hold furnace (1150 °C, 18 min), (**b**) Comparison of 70 and 85 mm slab DSPC austenite grain size leaving the holding furnace SF(1150 °C, 18 min), (**c**) the effect of holding temperature 1120 and 1150 °C on austenite size after leaving the holding furnace, and (**d**) the effect of holding time and temperature on austenite grain size after leaving the holding furnace.

Figure 13a shows that, for a DSPC 85 mm slab, austenite grain diameter increases from 50 μm to 784 μm on slab surface and from 1151 μm to 1391 μm in the slab center respectively. Extremely large austenite grains exist at the slab center before thermomechanical processing. Austenite grains coarsen much faster on the slab surface than in the slab center due to the larger driving force on the surface. Austenite grain size close to the center of the slab can be reduced from 1391 μm to 1161 μm by casting a 70 mm slab instead of 85 mm slab (Figure 13b). The effect of holding temperatures on austenite coarsening kinetics is shown in Figure 13c. Once again, the experimental measurement data are used as initial grain size, and the holding time, 18 min, is used for the calculation. The austenite grain size can be reduced from 1391 μm to 975 μm if increased secondary cooling is used, as well as, using the austenite nucleation density 12 during the delta ferrite to austenite phase transformation when casting an 85 mm slab. The effect of holding time at 1150 °C and 1120 °C is summarized in Figure 13d. The best combination to control austenite coarsening is to use increased secondary cooling during casting and set up the holding furnace at 1120 °C for 15 min, thus, the austenite grain size can be reduced from 1391 μm to 935 μm.

3.6. The Possibility of Producing New Alloy with Two-Phase Pinning

To refine HSLA steels austenite grain size during TSCDR process, carbides/nitrides of Ti, Nb and V are extensively used to retard grain growth at high temperatures [34,35]. However, these

precipitates are ineffective at pinning grain growth when the steel is held at a high temperature for long time due to fine particles dissolution and rapid particles coarsening. Zhou et al [36,37] proposed as a new steel system which can automatically pin the delta grain growth by using a small volume fraction of austenite phase at high temperature. The grain growth is controlled by the austenite phase coarsening rate which is determined by bulk diffusion.

Figure 14a shows the CON1D calculated temperature profile at the slab surface as well as those at 5 and 10 mm below the surface of an 85 mm, APIX70 slab, at Algoma Inc. using the DSPC process cast at a speed of 3.4 m/min. The recorded thermal profile obtained from the laboratory solidification experiment using the new Fe-Al model alloy (Table 1) is superimposed for comparison. The reordered cooling rates, using water quenching, forced air cooling, air cooling and in mould cooling used in lab processing are similar to the cooling rates calculated at slab surface, 5 mm, 10 mm below the surface, and the slab center of the TSDCR cast 85mm slab. In this way, one can compare the average grain sizes obtained from the solidification simulation tests to the grain-sizes measured at 0, 5, 10 mm below the surface and the center of the industrial slab. These comparisons are shown in Figure 14b, in which, the grain-size prior to entry into the soaking furnace was obtained by directly measuring the prior austenite grain size as a function of distance from the surface of the slab (Figure 2d). The data points for the new steel were positioned by matching the cooling rates in the solidification simulation test to the position at which these cooling rates would be observed within the slab. It can be seen that the expected grain size at the center would be 280 μm, compared to 1475 μm for APIX70, if the new steel was cast in the form of an 85 mm slab. This clearly demonstrates the potential advantage of this new alloy. One could also compare the grain-sizes within the APIX70 slab after exiting the soaking furnace, to those expected in the new alloy and observe that the grain size of the new alloy is essentially unchanged as a result of soaking which can prevent excessive grain growth prior to the onset of thermomechanical processing.

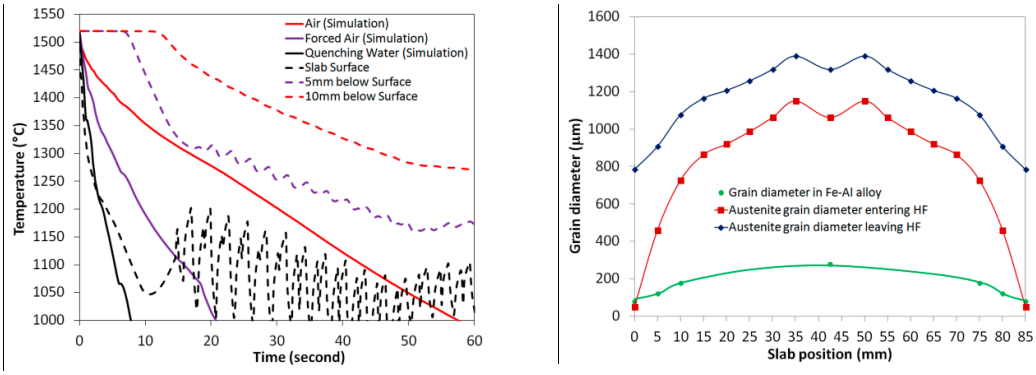

(**a**) (**b**)

Figure 14. (**a**) Comparison of CON1D predicted temperature profiles on the surface, 5 and 10 mm below the APIX70 85 mm slab and the recorded thermal profile during simulation process [37], (b) comparison of grain size evolution with slab distance using TSCDR process to produce APIX70 and Fe-Al% new alloy.

4. Conclusions

The developed grain growth model successfully reproduced grain growth as a function of position within the APIX70 slab in the TSCDR process. The results suggest that it is essential to control grain coarsening in each step from solidification to the holding furnace in order to maintain a required fine and uniform austenite grain size prior to the onset of thermomechanical processing.

Reducing the slab thickness can increase the cooling rate at the slab center during the TSCDR process. Predictions of the grain growth model suggest that austenite grain diameter can be reduced from 1345 μm to 500 μm if a 30 mm slab high cooling rate is produced. In addition, this would lead to less non-uniformity in the as-cast microstructure by refining the grains at the center of the slab. Increasing secondary cooling with restricted casting speed will increase cooling rate, resulting in

primary and secondary dendrite arm spacing refinement. Increased secondary cooling from 0.6 l/kg of hot steel to 1.4 l/kg of hot steel can reduce the grain size at the center of an 85mm thick slab from 1345 μm to 942 μm.

Liquid core reduction together with dynamic control of the liquid pool length can not only reduce center line segregation, solidification defects and porosity, but also provides the potential for generating more nucleation sites for delta ferrite resulting austenite grain refinement.

Increasing the number of austenite nucleation sites during the delta-ferrite to austenite phase transformation is an effective method of refining and homogenizing the as-cast microstructure of TSCDR microalloyed steels. When the Fe-1.5%Al alloy was deformed prior to the onset of the delta to gamma transformation austenite nucleated prolifically along the original delta grain boundaries and the newly recrystallized delta grain boundaries. The application of 20% deformation generated more than 30 recrystallized grains in each original delta grain. The calculations confirmed that the austenite grain in the 85 mm slab center can be reduced from 1345 μm to 1001 μm by doubling the nucleation sites.

Austenite grains continue grow inside the holding furnace. Optimizing the holding temperature and time can control austenite coarsening. The austenite grain size can be reduced from 1475 μm to 1072 μm if casting 70 mm slab with soaking temperature 1120 °C with 10 min instead of 1150 °C with 18 min.

The use of a delta-ferrite/austenite duplex microstructure is an effective method for pinning grain growth at high temperature. In the delta-ferrite/austenite duplex microstructure, the delta grain growth rate is very slow and controlled by the rate of coarsening of second phase particles. The developed grain growth model predicts that the delta grain size is 10 times smaller in duplex microstructure than that in materials without pinning. Laboratory validation shows that the delta grains are pinned throughout the TSCDR process, starting from the final stages of solidification. The concept of dual phase to retard grain coarsening as demonstrated by delta-ferrite/austenite duplex microstructure has great potential for producing more uniform as-cast microstructure for the TSCDR process.

Author Contributions: For research articles with several authors, a short paragraph specifying their individual contributions must be provided. The following statements should be used "conceptualization, Tihe Zhou, Hatem S. Zurob and Mani Subramanian; methodology, Tihe Zhou, Hatem S. Zurob, Mani Subramanian and Ronald J. O`Malley; software, Ronald J. O`Malley; validation, Tihe Zhou, Hatem S. Zurob and Ronald J. O`Malley; formal analysis, Tihe Zhou, Hatem S. Zurob and Ronald J. O`Malley ; investigation, Tihe Zhou, Hatem S. Zurob and Ronald J. O`Malley; resources, Sang-Hyun Cho and Peng Zhang; data curation, Tihe Zhou and Ronald J. O`Malley; writing—original draft preparation, Tihe Zhou; writing—review and editing, Ronald J. O`Malley and Mani Subramanian; visualization, Hatem S. Zurob; supervision, Hatem S. Zurob and Mani Subramanian; project administration, Mani Subramanian; funding acquisition, Mani Subramanian.

Funding: This research received no external funding.

Acknowledgments: The authors wish to acknowledge with thanks (i) technical support in making model alloys by CANMET (Hamilton, Canada), (ii) assistance in material characterization from Canadian Centre for Electron Microscopy (CCEM) at McMaster University (Hamilton, Canada) and (iii) the technological support from the DSPC operation team and New Product Development Department at Algoma Inc. (Sault Ste. Marie, Canada).

Conflicts of Interest: The authors declare no conflict of interest.

Appendix:

To calculate grain boundary mobility ***M(t)*** in Equation (2), the Turnbull mobility was used as an initial estimation:

$$M_{pure} = \frac{wD_{GB}\,V_m}{b^2RT}$$

In the above equation, w is the grain boundary thickness, D_{GB} is the grain boundary self-diffusion coefficient, $\boldsymbol{Vm}$ is the molar volume, $\boldsymbol{b}$ is the magnitude of the Burgers vector, R is the gas constant and T is the absolute temperature. The delta-ferrite has body-centered-cubic (BCC) crystal structure, the burgers vector is **b**=1/2<111> and $b = \sqrt{3}a/2$, where **a** is the lattice parameter of delta-ferrite, 0.286nm. The molar volume, $\boldsymbol{V_m}$=7.11cm^3. The activation energy for diffusion along the grain boundary was taken to be Q_{GB}=0.68Q where Q=256kJ/mole is the activation energy for bulk diffusion in BCC. Finally, w=1nm, and $Q_{GBo} = 1.67x10^{-4}\ m^3/s$. Given that Turnbull mobility does not take into account attachment kinetics, the grain boundary mobility in this way overestimates the experimental grain growth kinetics. The best fit of the experimental data was obtained using a mobility which is 1/3 of the Turnbull estimate [9]. Therefore, the delta grain mobility used in this work is:

$$M_{\delta}(t) = \frac{0.7075}{T(t)} \times \exp\left(\frac{-20,995.43}{T(t)}\right) \quad (3)$$

To estimate the mobility of the austenite grain boundaries, the austenite with face-centered cubic (FCC) crystal structure has **b**=1/2<110>, therefore, $b = \sqrt{2}a/2$, where a is 0.357nm. The molar volume, V_m is 6.85cm^3, the bulk diffusion activation energy in FCC Q=284kJ/mole, and that of grain boundary diffusion is: Q_{GB}=0.61Q. w=1nm, and$Q_{GBo} = 0.49x10^{-4}\ m^3/s$. Once again, the Turnbull mobility leads to an overestimation of the austenite grain growth kinetics. The best fit of the experimental data was obtained with a mobility which is 0.96 times the Turnbull estimate [9]. Thus, the austenite grain boundary mobility used in this calculation is:

$$M_{\gamma}(t) = \frac{0.3072}{T(t)} \times \exp\left(\frac{-20,837.14}{T(t)}\right) \quad (4)$$

The cooling path T(t) at each point of the slab and secondary dendrite arm spacing, thermophysical properties and spray heat transfer coefficients were calculated using CON1D V7.0 slab casting heat transfer model. The cast speeds for different slab thickness used in the simulations are listed as the following:

85 mm slab, casting speed 3.0-3.4 m/min,

70 mm slab, casting speed 3.4-4.0 m/min,

50 mm slab, casting speed 4.5-5.5 m/min,

30 mm slab, casting speed 4.5-6.5 m/min.

References

1. Klinkenberg, C.; Kintscher, B.; Hoen, K.; Reifferscheid, M. More than 25 Years of Experience in Thin Slab Casting and Rolling Current State of the Art and Future Developments. *Steel Research Int.* **2017**, *88(1)*, 1700272:1-10.
2. Arvedi, G.; Mazzolari, F.; Siegl, J.; Hohenbichler, G.; Holleis, G. Arvedi ESP first thin slab endless casting and rolling results. *Ironmak. Steelmak.* **2010**, *37*, 271-275.
3. Zhou, T.; Zhang, P.; Kuuskman, K.; Cerilli, E.; Cho, S.H.; Burella, D.; Zurob, S.H. Development of Medium-High Carbon Hot Rolled Steel Strip on a Thin Slab Casting Direct Strip Production Complex. *Ironmak & Steelmak*. **2018**, *45(7)*, 603-610.

4. Bhattacharya, D.; Misra, S. Development of Microalloyed Steels Through Thin Slab Casting and Rolling (TSCR) Route, *Transactions of the Indian Institute of Metals*. **2017**, *70(6)*, 1647–1659.
5. Challa, V.S.A.; Misra, R.D.K.; O'Malley, R.; Jansto, S.G. The Effect of Coiling Temperature on the Mechanical Properties of Ultrahigh-Strength 700 MPa Grade Processed via Thin-Slab Casting, AISTech 2014 Proceedings. Indianapolis, Ind., USA, May 5-8 2014, AIST **2014**, 2987-2997.
6. Nie, W.J.; Xin, W.F.; Xu, T.M.; Shi, P.J.; Zhang, X.B. Enhancing the Toughness of Heavy Thick X80 Pipeline Steel Plates by Microstructure Control. *Advanced Materials Research.* **2011**, *194-196*, 1183-1191.
7. Reip, C.P.; Hennig, W.; Kempken, J.; Hagmann, R. Development of CSP processed high strength pipe steels. *Mater Sci Forum.* **2005**, *500–501*, 287–294.
8. Wang, R.; Garcia, C.I.; Hua, M.; Zhang, H.; DeArdo, A.J. The Microstructure Evolution of Nb,Ti Complex Microalloyed Steel During the CSP Process. *Mater. Sci. Forum*. **2005**, *500–501*, 229–236.
9. Zhou, T.; O'Malley, R.J.; Zurob, H.S. Study of Grain-Growth Kinetics in Delta-Ferrite and Austenite with Application to Thin-Slab Cast Direct-Rolling Microalloyed Steels. *Metall. Mater. Trans. A.* **2010**, *41A*, 2112–2120.
10. Martin, J.W.; Doherty, R.D.; Cantor, B. *Stability of Microstructure in Metallic System*, Cambridge University Press, Cambridge, 1997, pp. 219-231.
11. Humphreys, F.J.; Hatherly, M. *Recrystallization and Related Annealing Phenomena*, 2nd ed., Elsevier Ltd., Oxford, UK, 2004,11-25.
12. Turnbull, D. Theory of grain boundary motion. *Trans. AIME*, **1951**, *191*, 661-665.
13. Köthe, A.; Kunze, J.; Backmann, G.; Mickel, C. Precipitation of TiN and (Ti,Nb)(C,N) during Solidification, Cooling and Hot Direct Deformation. *Mater Sci Forum*. **1998**, *284-286*, 493-500.
14. Nagata, M.T.; Speer, J.G.; Matlock, D.K. (2002). Titanium Nitride Precipitation Behavior in Thin-Slab Cast High-Strength Low-Alloy Steels. *Metall. Mater. Trans. A*. 2002, *33A*, 3099-3109.
15. Smith, C.S. Grains, Phases, and Interfaces: An Interpretation of Microstructure, *Trans. Metall. Soc. A. I. M. E.* **1948,** *175*, 15-51.
16. Kwon, O.; DeArdo, A.J. Interactions between Recrystallization and Precipitation in Hot-deformed Microalloyed steels. *Acta Metall*. **1991**, *39(4)*, 529-538.
17. Palmiere, E.J.; Garcia, C.I.; DeArdo, A.J. Compositional and Microstructural Changes Which Attend Reheating and Grain Coarsening in Steels Containing Niobium. *Metall. Mater. Trans. A*. **1994**, *25A*, 277-286.
18. Poths, R.M.; Rainforth, W.M.; Palmiere, E.J. Strain Induced Precipitation in Model and Conventional Microalloyed Steels during Thermomechanical Processing. *Mater Sci Forum*. **2005,** *500-501*, 139-145.
19. Zurob, H.S.; Hutchinson, C.R.; Brechet, Y.; Purdy, G. Modeling recrystallization of microalloyed austenite: effect of coupling recovery, precipitation and recrystallization. *Acta Mater*. **2002**, *50*, 3075-3092.
20. Gladman, T. *The Physical Metallurgy of Microalloyed Steel*. Institute of Metals, London, UK, 1997.
21. Available from Thermo-calc Software: www.thermocalc.com.
22. Meng, Y.; Thomas, B.G. Heat-Transfer and Solidification Model of Continuous Slab Casting: CON1D. *Metall. Mater. Trans. B.* **2003**, *34B*, 685-705.
23. Yin, H.; Emi, T.; Shibara, H. Morphological Instability of δ-Ferrite/γ-Austenite Interphase Boundary in Low Carbon Steel. *Acta Mater*. **1999**, *47(5)*, 1523-1535.
24. Kim, H.S.; Kobayashi, Y.; Nagai, K. Prediction of Prior Austenite Grain Size of High-phosphorous Steels through Phase Transformation Simulation. *ISIJ Int.* **2006**, *46(6)*, 854-858.
25. Holzhauser, J.F.; Spitzer, K.H.; Schweredtfeger, K. Study of Heat Transfer Though Layers of Casting Flux: Experiments with a Laboratory Set-up Simulating the Conditions in Continuous Casting. *Steel Research*. **1999,** *70(7)*, 252-257.
26. Gonzalez, M.; Goldschmit, M.B.; Assanelli, A.P.; Berdaguer, E.F.; Dvorkin, E. Modeling of the Solidification Process in a Continuous Casting Installation for Steel Slabs. *Metall. Mater. Trans. B.* **2003**, *34B(8)*, 455-473.
27. Louhenkilpi, S.; Makinen, M.; Vapalahti, S.; Raisanen, T.; Laine, J. 3D Steady State and Transient Simulation Tools for Heat Transfer and Solidification in Continuous Casting. *Mater. Sci. and Eng. A*. **2005**, *413-414*, 135-138.
28. Sobral, M.D.C.; Mei, P.R.; Santos, R.G.; Gentile, F.C.; Bellon, J.C. Laboratory simulation of thin slab casting. *Ironmak Steelmak*. **2003**, *30*, 412–416.
29. Zhou, T.H.; Gheribi, A.E.; Zurob, H.S. Austenite particle coarsening and delta-ferrite grain growth in model Fe-Al alloy. *Can. Metall. Q*. **2013**, *52(1)*, 90-97.

30. McCarrney, D.G.; Hunt, J.D. Measurements of cell and primary dendrite arm spacing in directionally solidified aluminum alloys. *Acta Metall*. **1981**, *29*,1851–1863.
31. Bouchard, D.; Kirkaldy, J.S. Prediction of dendrite arm spacings in unsteady and steady-state heat flow of unidirectionally solidified binary alloys. *Metall. Mater. Trans. B*. **1997**, *28B*, 651–663.
32. Taha, M.A. Influence of solidification parameters on dendrite arm spacings in low carbon steels. *J Mater Sci Lett*. **1986**, *5*, 307–310.
33. Cahn, R.W.; Haasen, P. *Physical metallurgy*. 4th ed. Amsterdam: North-Holland Physics Publishing; 1996.
34. Zhou, T.; Overby, D.; Badgley, P.; Martin-Root, C.; Wang, X.; Liang, S.L.; Zurob, S.H. Study of processing, microstructure and mechanical properties of hot rolled ultra high strength steel. *Ironmak & Steelmak*, **2018**, doi.org/10.1080/03019233.2018.1468652.
35. Hillert, M. Inhibition of Grain Growth by Second-Phase Particles. *Acta Metall*. **1988**, *36*, 3177-3181.
36. Zhou, T.; Zurob, S.H.; O'Malley, R.J.; Rehman, K. Model Fe-Al Steel with Exceptional Resistance to High Temperature Coarsening. Part I: Coarsening Mechanism and Particle Pinning Effects. Metall. *Mater. Trans. A*. **2015**, *41A*, 178-189.
37. Zhou, T.; Zhang, P.; O'Malley, R.J.; Zurob, S.H.; Subramanian M. Model Fe-Al Steel with Exceptional Resistance to High Temperature Coarsening. Part II: Experimental Validation and Applications. *Metall. Mater. Trans. A*, **2015**, *41A*, 190-198.